Dynamics and thermalization in a simple mesoscopic fermionic bath

Michael Mwalaba,[1,2,*] Ilya Sinayskiy,[1,3,†] and Francesco Petruccione[1,3,4,‡]

[1]*Quantum Research Group, School of Chemistry and Physics, University of KwaZulu-Natal, Durban, KwaZulu-Natal, 4001, South Africa*

[2]*Department of Physics, School of Natural Sciences, University of Zambia, Lusaka 10101, Zambia*

[3]*National Institute for Theoretical Physics (NIThePh), KwaZulu-Natal, 4001, South Africa*

[4]*School of Electrical Engineering, KAIST, Daejeon, 34141, Republic of Korea*

(Received 11 May 2018; published 1 May 2019)

We consider a central fermion strongly interacting with a surrounding mesoscopic bath of fermions which is weakly coupled to a Markovian bath of fermions. The master equation of the system consisting of the central fermion and the mesoscopic bath is derived, and based on this master equation, the reduced dynamics and thermalization of the central fermion are investigated. As probes for studying the dynamics and thermalization, the mean number of the central fermion and the current density are calculated. The observed dynamics reveal that strong coupling strength induces non-Markovian behavior and that in the long time limit thermalization is attained leaving the central fermion in a thermal state that is described by the corresponding Gibbs distribution. Upon attaining the thermal state, the central fermion is found to be entangled with the collective mode of the surrounding mesoscopic bath in the high-temperature regime, whereas in the low-temperature regime, it is found to undergo sudden death of entanglement.

DOI: 10.1103/PhysRevA.99.052102

I. INTRODUCTION

Investigations of the influence of the environment on the dynamics of open quantum systems is an active area of research [1–8]. As physical implementations of quantum systems are increasingly becoming widespread, these investigations become fundamentally crucial since these implementations imply exposing the quantum system to the environment. Also in nature quantum systems are never completely isolated from their environment. In modeling open quantum systems, the nature of the environment can, in general, vary (either fermionic [9–11] or bosonic [12]) depending on what one seeks to model. Paradigmatic examples of such models are the Fano-Anderson model [13], the spin-boson model [1,14,15], and the Caldeira-Leggett model [1,15,16].

These investigations have revealed that a characteristic feature of an open quantum system is that in the course of undergoing its dynamics, the reduced system loses information to the environment. This phenomenon has been coined decoherence and it is known to pose a serious challenge to physical implementations such as quantum information processing [17]. Furthermore, the flow of information to the environment is either unidirectional or bidirectional. The corresponding dynamics have been termed Markovian and non-Markovian dynamics, respectively. Exactly what determines the direction of information has attracted a great deal of attention. Various works [2,3,5,8,18] suggest the onset of non-Markovian dynamics from Markovian dynamics when one switches the coupling strength from weak to strong. In applications such as quantum information processing, reservoir engineering [19–22], and quantum technologies, it is very important to know exactly what kind of dynamics (Markovian or non-Markovian) the quantum system will undergo for a given regime of parameters because certain characteristic quantum properties are robust when the dynamics is of a specific kind. For example, entanglement is known to be long lived when the dynamics is non-Markovian [23].

In this work, we seek to investigate the emergence of non-Markovian dynamics from Markovian dynamics and the ensuing thermalization [12,24–28] and entanglement of formation of a system of fermions. We note that a survey of existing literature reveals several measures of non-Markovianity [18,19,29–33] which are all based on nonmonotonic behavior, but we will use the Breuer-Laine-Piilo (BLP) measure of non-Markovianity as suggested by Breuer and co-workers [18]. We consider a system consisting of a fermion of interest sitting at the radial center of a mesoscopic bath consisting of a finite number of fermions sitting in a circular configuration of occupation sites. Due to the Pauli exclusion principle, each site in the system is occupied by a maximum of one fermion. The system is embedded in a Markovian bath [1] of fermions with which each of the mesoscopic fermions is weakly interacting; see Fig. 1. All fermions in the system are spinless and the interaction between the mesoscopic fermions is considered negligible compared to the interaction between the fermion of interest and each of the fermions in the mesoscopic bath. The latter is taken to be strong and uniform throughout. Thus, the mesoscopic bath is collective. Numerous studies of collective atomic dynamics in connection with fermions, spins, atomic clocks, and quantum information have been done [8,17,34,35]. Symmetric configurations like this are known to yield master equations that are exactly solvable [18,36]. The advantages of this model is that, while displaying several

*micmwalaba@gmail.com
†sinayskiy@ukzn.ac.za
‡petruccione@ukzn.ac.za

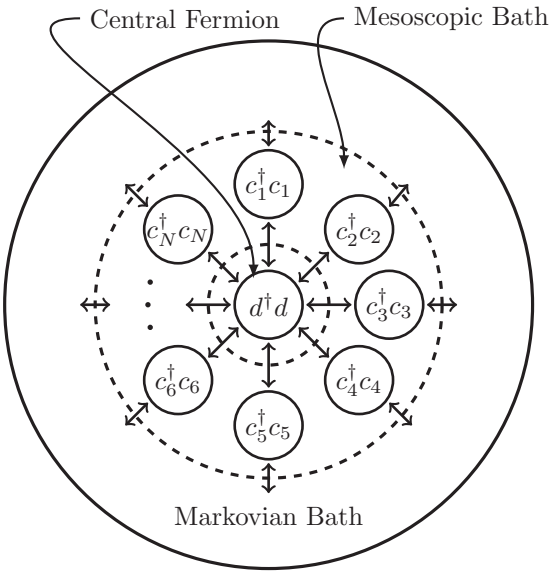

FIG. 1. Central fermion of interest $d^\dagger d$ strongly interacting with a surrounding fermionic mesoscopic bath which is weakly interacting with a fermionic Markovian bath.

interesting features like dissipation, decoherence, thermalization, entanglement, Markovian, and non-Markovian behavior, it is analytically solvable and it can be actually mimicked in experiments with ultracold fermionic atoms in single center traps or optical lattices due to the presence of a single or many geometrical centers, respectively, around which atoms are usually trapped. Spinless fermions are also readily available in the form of spinless fermionic atoms [37–43].

The paper is structured as follows. In Sec. II we start from the general quantum master equation in the Born-Markov approximation to derive the master equation of the reduced system consisting of the fermion of interest and the mesoscopic bath. We move on to solve the derived master equation giving us the reduced density matrix from which we obtain the density matrix of the fermion of interest by tracing out the degrees of freedom of the mesoscopic bath. This is followed in Sec. III A by calculations of the mean number of the fermion of interest, the current density and measure of non-Markovianity which we use to observe the dynamics and thermalization. We then show analytically that thermalization is achieved in Sec. III B. In Sec. III C, we analyze thermal entanglement between the fermion of interest and the collective fermionic mode of the mesoscopic bath. We finally summarize and conclude in Sec. IV.

II. MODEL AND QUANTUM MASTER EQUATION

The studied system consists of a fermion strongly interacting with a mesoscopic bath of fermions which is embedded in a Markovian fermionic bath. The total Hamiltonian reads

$$H = H_S + H_B + H_{SB}, \tag{1}$$

where H_S is the Hamiltonian of the fermion of interest strongly interacting with the mesoscopic bath, i.e.,

$$H_S = \omega d^\dagger d + \sum_{i=1}^{N} (\epsilon c_i^\dagger c_i + g c_i^\dagger d + g d^\dagger c_i), \tag{2}$$

where we have collectively called the fermion of interest, the mesoscopic bath, and the interaction between them the system because they are strongly interacting; $d^\dagger, d$ are creation and annihilation operators of the fermion of interest satisfying the standard anticommutation relations,

$$\{d, d^\dagger\}_+ = 1, \quad \{d, d\}_+ = 0, \quad \{d^\dagger, d^\dagger\}_+ = 0, \tag{3}$$

and $c_i^\dagger, c_i$ are creation and annihilation operators of the fermions in the mesoscopic bath satisfying the standard anticommutation relations,

$$\{c_i, c_j^\dagger\}_+ = \delta_{ij}, \quad \{c_i, c_j\}_+ = 0, \quad \{c_i^\dagger, c_j^\dagger\}_+ = 0. \tag{4}$$

The Hamiltonian H_B of the Markovian bath reads

$$H_B = \sum_n \omega_n b_n^\dagger b_n, \tag{5}$$

where $b_n^\dagger, b_n$ are standard fermionic creation and annihilation operators satisfying the standard anticommutation relations,

$$\{b_n, b_m^\dagger\}_+ = \delta_{nm}, \quad \{b_n, b_m\}_+ = 0, \quad \{b_n^\dagger, b_m^\dagger\}_+ = 0. \tag{6}$$

As can be seen, Eq. (3), Eq. (4), and Eq. (6) are satisfied by operators belonging to the same subsystem whereas operators belonging to different subsystems anticommute regardless of conjugation, e.g.,

$$\{b_n, c_i^\dagger\}_+ = 0, \quad \{b_n, d\}_+ = 0, \quad \{c_i^\dagger, d^\dagger\}_+ = 0. \tag{7}$$

The Hamiltonian of interaction between the mesoscopic bath and the Markovian bath is denoted by H_{SB} and in the rotating wave approximation [1,44] is given by

$$H_{SB} = \sum_{i=1}^{N} \sum_n g_n c_i^\dagger b_n + g_n^* b_n^\dagger c_i. \tag{8}$$

Using the fact that the Hamiltonian of the system H_S, Eq. (2), is quadratic in form, it can be diagonalized so that it becomes

$$H_S = \sum_{i=0}^{N} \lambda_i \xi_i^\dagger \xi_i, \tag{9}$$

where $\xi_i^\dagger, \xi_i$ are creation and annihilation operators of a new set of quasifermions satisfying standard anticommutation relationships,

$$\{\xi_i, \xi_j^\dagger\}_+ = \delta_{ij}, \quad \{\xi_i, \xi_j\}_+ = 0, \quad \{\xi_i^\dagger, \xi_j^\dagger\}_+ = 0. \tag{10}$$

The explicit expressions for the quasifermionic operators $\xi_i^\dagger$ and their corresponding quasienergies λ_i read

$$\xi_0^\dagger = \sin\theta c^\dagger + \cos\theta d^\dagger, \quad \lambda_0 = \frac{\omega + \epsilon}{2} + \frac{\Omega_N}{2}, \tag{11}$$

$$\xi_1^\dagger = \cos\theta c^\dagger - \sin\theta d^\dagger, \quad \lambda_1 = \frac{\omega + \epsilon}{2} - \frac{\Omega_N}{2}, \tag{12}$$

$$\xi_i^\dagger = \sqrt{\frac{i-1}{i}} c_i^\dagger - \frac{1}{\sqrt{i(i-1)}} \sum_{k=1}^{i-1} c_k^\dagger, \quad \lambda_i = \epsilon, \tag{13}$$

where $i = 2, 3, \ldots, N$, and

$$\Omega_N = \sqrt{4g^2N + (\epsilon - \omega)^2}, \tag{14}$$

$$\theta = \frac{1}{2}\tan^{-1}\left(\frac{2g\sqrt{N}}{\omega - \epsilon}\right), \tag{15}$$

$$c = \frac{1}{\sqrt{N}}\sum_{i=1}^{N} c_i. \tag{16}$$

Calculating the anticommutator of the operator c appearing in Eq. (16), we get

$$\{c, c^\dagger\}_+ = 1, \tag{17}$$

which means that the whole mesoscopic bath behaves effectively like a single collective fermionic mode. The implication of this is that the system consisting of the fermion of interest and N fermions in the mesoscopic bath is effectively transformed into a simpler system consisting of the fermion of interest d and an effective mesoscopic fermion c. We attribute this implication to result from the symmetry of the system. By combining Eq. (11) and Eq. (12), we see that the transformation equations from the original picture to the quasifermionic picture are given by

$$d = \cos\theta\xi_0 - \sin\theta\xi_1, \tag{18}$$

$$c = \sin\theta\xi_0 + \cos\theta\xi_1, \tag{19}$$

so that in the quasifermionic picture the interaction Hamiltonian, Eq. (8), becomes

$$H_{SB} = \sqrt{N}\sum_n g_n b_n(\sin\theta\xi_0^\dagger + \cos\theta\xi_1^\dagger) + g_n^*(\sin\theta\xi_0 + \cos\theta\xi_1)b_n^\dagger, \tag{20}$$

and the total Hamiltonian, Eq. (1), therefore can be written as

$$H = \sum_{i=0}^{N}\lambda_i\xi_i^\dagger\xi_i + \sum_n \omega_n b_n^\dagger b_n + \sqrt{N}\sum_n g_n b_n(\sin\theta\xi_0^\dagger + \cos\theta\xi_1^\dagger) + g_n^*(\sin\theta\xi_0 + \cos\theta\xi_1)b_n^\dagger. \tag{21}$$

Switching to the interaction picture, the interaction Hamiltonian Eq. (20) attains the form,

$$H_{SB}^{(I)}(t) = \xi_0^\dagger B_{0t} + \xi_1^\dagger B_{1t} + \text{H.c.}, \tag{22}$$

where

$$B_{0t} = \sqrt{N}\sum_n g_n \sin\theta e^{it(\omega_n - \lambda_0)}b_n, \tag{23}$$

$$B_{1t} = \sqrt{N}\sum_n g_n \cos\theta e^{-it(\omega_n - \lambda_1)}b_n, \tag{24}$$

and H.c. symbolizes the Hermitian conjugate of the two terms appearing in Eq. (22).

The starting point for the derivation of the quantum master equation for the reduced system is the general expression for the quantum master equation in the Born-Markov approximation [1],

$$\dot{\rho}_S(t) = -\int_0^\infty d\tau \text{Tr}_B\left[H_{SB}^{(I)}(t), \left[H_{SB}^{(I)}(t-\tau), \rho_S(t)\otimes\rho_B(0)\right]\right]. \tag{25}$$

Substituting the interaction Hamiltonian Eq. (22) into Eq. (25) and taking the simple case where $|\lambda_0 - \lambda_1| \gg 1$ which holds for $N \gg 1$, we obtain the following quantum master equation,

$$\dot{\rho}_S(t) = \sum_{i=0}^{1}\gamma_i^+\left(\xi_i\rho_S\xi_i^\dagger - \frac{1}{2}\{\xi_i^\dagger\xi_i, \rho_S\}_+\right) + \gamma_i^-\left(\xi_i^\dagger\rho_S\xi_i - \frac{1}{2}\{\xi_i\xi_i^\dagger, \rho_S\}_+\right), \tag{26}$$

where the damping rates $\gamma_i^\pm$ are given by

$$\gamma_0^\pm = \pi N\sin^2\theta J(\lambda_0)\left(1 \pm \tanh\frac{\beta\lambda_0}{2}\right), \tag{27}$$

$$\gamma_1^\pm = \pi N\cos^2\theta J(\lambda_1)\left(1 \pm \tanh\frac{\beta\lambda_1}{2}\right), \tag{28}$$

where β is the inverse temperature of the fermionic Markovian bath and $J(\lambda_i)$ is the spectral density [1] obtained from the substitution $\sum_n |g_n|^2 \to \int d\omega J(\omega)\delta(\omega_n - \omega)$ where $J(\omega) = \frac{\gamma}{2\pi}\frac{\Gamma^2}{(\omega-\omega_0)^2+\Gamma^2}$ is the Lorenztian spectral density.

To solve the above quantum master equation, Eq. (26), we can use the Kraus representation [17,45,46] which in combination with the fact that superoperators corresponding to $i = 0$ and $i = 1$ in Eq. (26) commute [i.e., Eq. (26) can also be written in the form $\dot{\rho}_S = (\mathcal{L}_0 + \mathcal{L}_1)\rho_S$ where superoperators satisfy the relation $[\mathcal{L}_0, \mathcal{L}_1] = 0$)] allows us to obtain

$$\rho_S(t) = e^{t\mathcal{L}_0}e^{t\mathcal{L}_1}\rho_S(0) = e^{t\mathcal{L}_1}e^{t\mathcal{L}_0}\rho_S(0) = \sum_{j,k=0}^{3}E_{j0}(t)E_{k1}(t)\rho_S(0)E_{k1}^\dagger(t)E_{j0}^\dagger(t), \tag{29}$$

as the solution of the quantum master equation, Eq. (26), in the Kraus representation, where we derive the Kraus operators to be

$$\begin{aligned} E_{0i}(t) &= \cos(\alpha_i)(\xi_i^\dagger\xi_i + f_i(t)\xi_i\xi_i^\dagger), \\ E_{1i}(t) &= \cos(\alpha_i)g_i(t)\xi_i^\dagger, \\ E_{2i}(t) &= \sin(\alpha_i)(\xi_i\xi_i^\dagger + f_i^*(t)\xi_i^\dagger\xi_i), \\ E_{3i}(t) &= \sin(\alpha_i)g_i(t)\xi_i, \end{aligned} \tag{30}$$

with

$$\cos(\alpha_i) = \sqrt{\frac{\gamma_i^-}{\gamma_i^\beta}} = \sqrt{\frac{1}{1+e^{\beta\lambda_i}}} = \sqrt{p_i}, \tag{31}$$

$$\sin(\alpha_i) = \sqrt{\frac{\gamma_i^+}{\gamma_i^\beta}} = \sqrt{1 - \frac{1}{1+e^{\beta\lambda_i}}} = \sqrt{1-p_i}, \tag{32}$$

$$f_i(t) = \exp\left(-\frac{\gamma_i^\beta}{2}t - i\lambda_i t\right), \tag{33}$$

$$g_i(t) = \sqrt{1 - |f_i(t)|^2}, \tag{34}$$

$$\gamma_i^\beta = \gamma_i^+ + \gamma_i^-. \tag{35}$$

The Kraus operators are subject to the normalization condition,

$$\sum_{j,k=0}^{M} E_{k1}^{\dagger}(t)E_{j0}^{\dagger}(t)E_{j0}(t)E_{k1}(t) = I. \tag{36}$$

The above solution of the quantum master equation, Eq. (29), is valid for arbitrary initial conditions. We can express the arbitrary initial conditions in the general form,

$$\rho_S(0) = \rho_{00}(0)\xi_0^{\dagger}|0\rangle\langle 0|\xi_0 + \rho_{01}(0)\xi_0^{\dagger}|0\rangle\langle 0|\xi_1 + \rho_{10}(0)\xi_1^{\dagger}|0\rangle\langle 0|\xi_0 + \rho_{11}(0)\xi_1^{\dagger}|0\rangle\langle 0|\xi_1, \tag{37}$$

where the coefficients $\rho_{00}(0)$, $\rho_{01}(0)$, $\rho_{10}(0)$, and $\rho_{11}(0)$ are arbitrary subject to the normalization condition,

$$\rho_{00}(0) + \rho_{11}(0) = 1. \tag{38}$$

Using this arbitrary initial density matrix of the system, Eq. (37), in the general solution, Eq. (29), and tracing out the degrees of freedom of the mesoscopic bath, we obtain the density matrix of the fermion of interest,

$$\rho(t) = \mathrm{Tr}_c[\rho_S(t)] = \kappa(t)d^{\dagger}|0\rangle\langle 0|d + (1-\kappa(t))|0\rangle\langle 0|, \tag{39}$$

where

$$\kappa(t) = n_0(t)\rho_{00}(0) + n_1(t)\rho_{11}(0) + \tilde{n}_2(t)\rho_{10}(0), \tag{40}$$

with $n_0(t)$, $n_1(t)$, and $\tilde{n}_2(t)$ being given by

$$\begin{aligned} n_0(t) &= p_0 + |f_0|^2(\cos^2\theta(1-p_0p_1) - p_0), \\ n_1(t) &= p_1 + |f_1|^2(\sin^2\theta(1-p_0p_1) - p_1), \\ \tilde{n}_2(t) &= -2\mathrm{Re}(f_0(t)f_1^*(t))\sin\theta\cos\theta. \end{aligned} \tag{41}$$

In Eq. (41), $\mathrm{Re}(f_0(t)f_1^*(t))$ means the real part of the product of $f_0(t)$ and $f_1^*(t)$. In principle, the density matrix given by Eq. (39) can be used to calculate various properties of the fermion of interest for arbitrary initial conditions subject to the normalization condition Eq. (38).

III. RESULTS AND DISCUSSION

In this section, we will investigate various features of the reduced system and the fermion of interest. In Sec. III A, we investigate the dynamics in terms of the mean number of fermions, current density, BLP measure of non-Markovianity, and von Neumann entropy. In Sec. III B, we investigate thermalization and in Sec. III C we investigate entanglement of formation to analyze entanglement between the fermion of interest and the collective mesoscopic fermion.

A. Dynamics of the fermion of interest

To investigate the dynamics of the fermion of interest we are going to calculate its mean number. Based on the exact expression for the reduced density matrix of the fermion of interest, Eq. (39), we obtain the mean number of the fermion of interest to be

$$n(t) = \langle d^{\dagger}d\rangle = \mathrm{Tr}[d^{\dagger}d\rho(t)] = \kappa(t), \tag{42}$$

where $\kappa(t)$ is given above, Eq. (40). In the present work we will consider that initially there is only one fermion of interest and no fermions in the mesoscopic bath, i.e.,

$$\rho_S(0) = d^{\dagger}|0\rangle\langle 0|d. \tag{43}$$

We can express this particular initial condition, Eq. (43), in the form of the general expression in Eq. (37) by using the transformation equation, Eq. (18), so that it appears as

$$\rho_S(0) = \cos^2\theta\,\xi_0^{\dagger}|0\rangle\langle 0|\xi_0 - \sin\theta\cos\theta\,\xi_0^{\dagger}|0\rangle\langle 0|\xi_1 - \sin\theta\cos\theta\,\xi_1^{\dagger}|0\rangle\langle 0|\xi_0 + \sin^2\theta\,\xi_1^{\dagger}|0\rangle\langle 0|\xi_1. \tag{44}$$

By comparing Eq. (44) and Eq. (37), we identify $\rho_{00}(0) = \cos^2\theta$, $\rho_{11}(0) = \sin^2\theta$, and $\rho_{01}(0) = \rho_{10}(0) = -\sin\theta\cos\theta$ so that the mean number of the fermion of interest, Eq. (42), explicitly appears as

$$n(t) = n_0(t)\cos^2\theta + n_1(t)\sin^2\theta + n_2(t), \tag{45}$$

where

$$n_2(t) = 2\mathrm{Re}(f_0(t)f_1^*(t))\sin^2\theta\cos^2\theta. \tag{46}$$

As a further investigation of the dynamics, we will measure the flow of the fermion of interest between the site of interest and the mesoscopic bath. To this end, we use the total density matrix of the system Eq. (29) and the transformation equations, Eq. (18) and Eq. (19), to calculate the current density,

$$\begin{aligned} J(t) &= -i\langle c^{\dagger}d - d^{\dagger}c\rangle \\ &= \sin 2\theta\{\mathrm{Im}(f_0)\mathrm{Re}(f_1) - \mathrm{Re}(f_0)\mathrm{Im}(f_1)\} \\ &= \sin 2\theta\exp\left(-\frac{\gamma_0^{\beta}+\gamma_1^{\beta}}{2}t\right)\sin(\Omega_N t), \end{aligned} \tag{47}$$

where $\mathrm{Re}(f_i)$ and $\mathrm{Im}(f_i)$ correspond to the real and imaginary parts of f_i, respectively.

In what follows, we will plot graphs to show our investigation of the behavior of the mean number of the fermion of interest $n(t)$ and the current density $J(t)$ with time for different values of the coupling strength between the fermion of interest and the mesoscopic bath, for different values of the number of fermions in the mesoscopic bath, and for different temperatures of the Markovian bath. The investigation of the behavior of the mean number of the fermion of interest and current density with time for different values of the coupling strength will be done concurrently with the investigation of the BLP measure of non-Markovianity [18] which in this work appears as

$$\begin{aligned} \mathcal{N}(t) &= \max_{\rho^{(1)}(0),\rho^{(2)}(0)} D(\rho^{(1)},\rho^{(2)}) \\ &= \max_{\rho^{(1)}(0),\rho^{(2)}(0)} \sqrt{\left(\rho_{11}^{(1)} - \rho_{11}^{(2)}\right)^2 + \left|\rho_{01}^{(1)} - \rho_{01}^{(2)}\right|^2}. \end{aligned} \tag{48}$$

Noting from Eq. (39) that $\rho_{11} = \kappa(t)$ and $\rho_{01} = 0$ and performing the maximum over all initial states of the system as suggested in [47], Eq. (48) becomes

$$\mathcal{N}(t) = |n_0(t)| + |n_1(t)| + 2\sqrt{2}|\tilde{n}_2(t)|. \tag{49}$$

In Fig. 2, we analyze different regimes of the interaction between the fermion of interest and fermions in the mesoscopic bath. From top to bottom the values of the coupling strength g are 0.1, 1.0, and 2.0, respectively, while the rest of the parameters are chosen to be the same for all

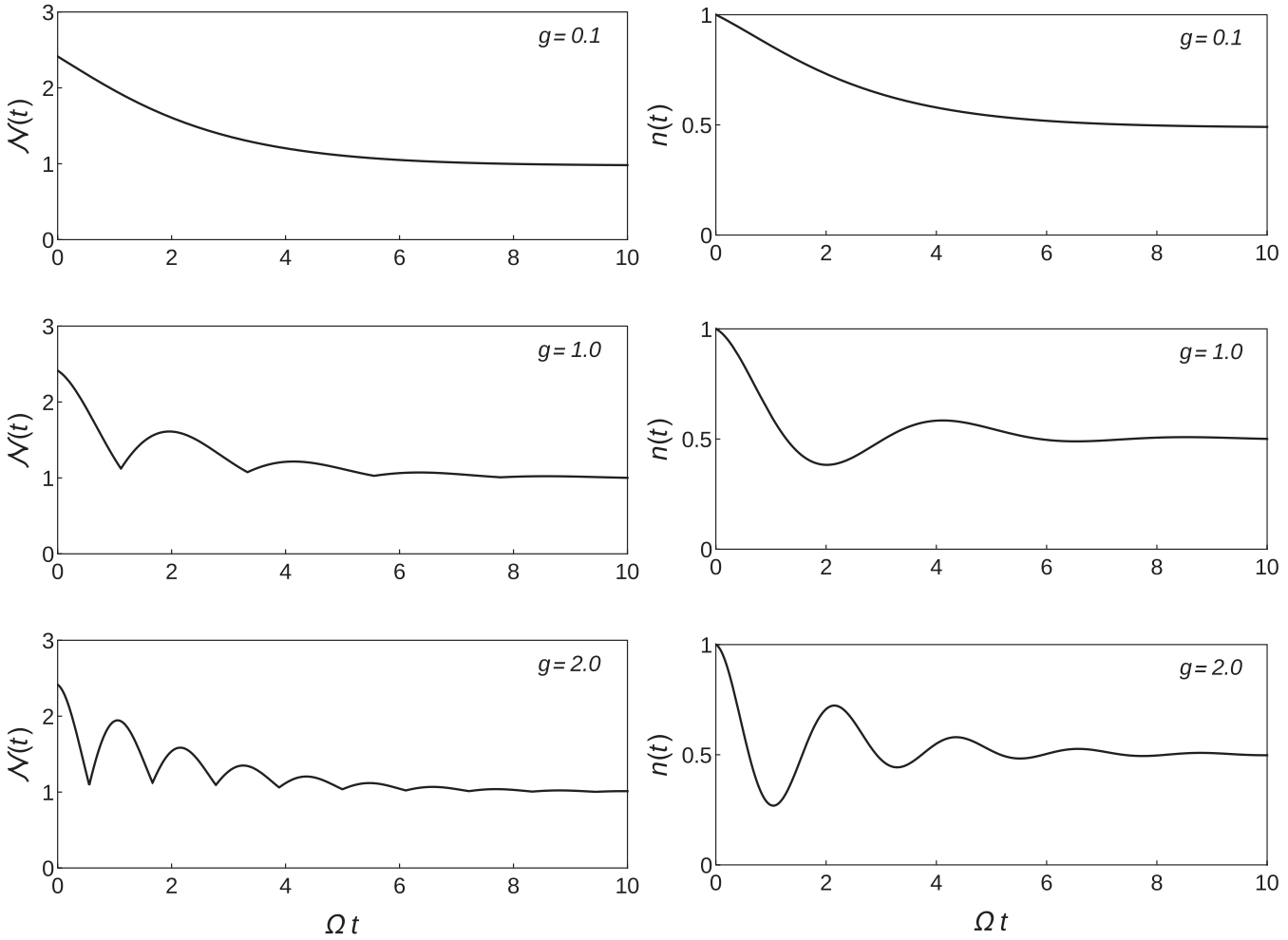

FIG. 2. Time dependence of measure of non-Markovianity $\mathcal{N}(t)$ and mean number of fermion of interest $n(t)$ for different values of coupling strength g to the mesoscopic bath; t is time measured in units of Ω^{-1} so that Ωt in the abscissa is dimensionless. The rest of the parameters are chosen to be the same for all curves: $\epsilon = 1$, $\omega = 1.3$, $N = 5000$, $\Omega = \frac{\gamma}{2} = \pi J(\lambda_0) = \pi J(\lambda_1) = 10^{-6}$, and $\beta = 1$. It is clear that when the interaction strength is weak, both $\mathcal{N}(t)$ and $n(t)$ are monotonically decreasing functions until thermalization is attained. As the interaction strength is increased, we observe that both $\mathcal{N}(t)$ and $n(t)$ start to oscillate with the oscillations getting severe in the strong coupling regime. Since the measure of non-Markovianity measures the degree of non-Markovianity, we can therefore say that the interaction strength controls the nature of the dynamics, whether Markovian or non-Markovian.

three curves: $\epsilon = 1$, $\omega = 1.3$, $N = 5000$, $\Omega = \frac{\gamma}{2} = \pi J(\lambda_0) = \pi J(\lambda_1) = 10^{-6}$, and $\beta = 1$. It is clear that in the weak coupling case ($g = 0.1$ and other values lower than this value not shown in Fig. 2 to avoid redundancy), a monotonically decreasing curve which is typical of Markovian dissipation [5,18] is observed. According to [18], such a curve for the measure of non-Markovianity means that there is no backflow. The curve for the mean number decays to a constant value of approximately 0.5 and remains there for longer times giving us signs of thermalization. As the interaction strength is increased, the curves slowly begin to oscillate ($g = 1.0$ curves) with increased oscillations for larger interaction strength (e.g., $g = 2.0$ curve). The oscillations indicate that the electron tunnels back and forth between the site of interest and the mesoscopic bath. The mean number of the thermal state of 0.5 is a reasonable prediction because the system contains a single electron which, as time approaches infinity, is averaged by the two subsystems between which it is oscillating. Thus, in increasing the interaction strength, the process of thermalization shows clear signs of non-Markovian behavior.

Similarly, in Fig. 3, we analyze the current density for different regimes of the interaction between the fermion of interest and fermions in the mesoscopic bath. From top to bottom the values of the coupling strength g are 0.1, 1.0, and 2.0, respectively, while the rest of the parameters are chosen to be the same for all three curves: $\epsilon = 1$, $\omega = 1.3$, $N = 5000$, $\Omega = \frac{\gamma}{2} = \pi J(\lambda_0) = \pi J(\lambda_1) = 10^{-6}$, and $\beta = 1$. For the weakest coupling ($g = 0.1$) the current curve moves only very slightly from $J(t = 0) = 0$ to a negative value of $J(t)$ and then goes back to $J(t) = 0$ for all longer times. The curve for the measure of non-Markovian shows no oscillations, hence no backflow. As the interaction strength is increased, the curves slowly begins to oscillate ($g = 1.0$ curve) with increased oscillations for larger interaction strength (e.g., $g = 2.0$ curve). This once again shows that in increasing the interaction strength the process of thermalization displays signs of non-Markovian behavior.

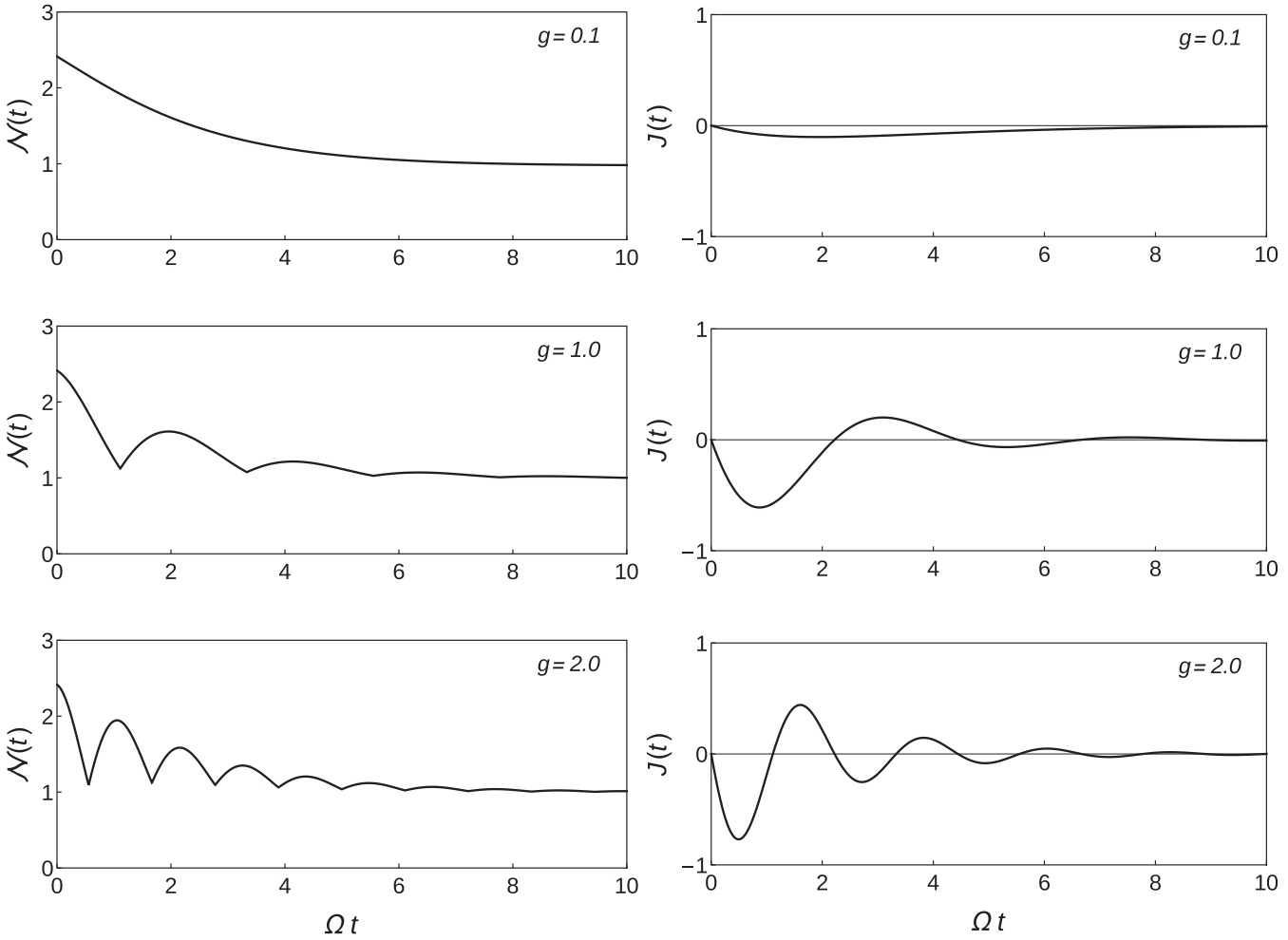

FIG. 3. Time dependence of measure of non-Markovianity $\mathcal{N}(t)$ and current $J(t)$ for different values of coupling strength g to the mesoscopic bath; t is time measured in units of Ω^{-1} so that Ωt in the abscissa is dimensionless. The rest of the parameters are chosen to be the same for all curves: $\epsilon = 1$, $\omega = 1.3$, $N = 5000$, $\Omega = \frac{\gamma}{2} = \pi J(\lambda_0) = \pi J(\lambda_1) = 10^{-6}$, and $\beta = 1$. It is clear that as the interaction strength is increased, we observe that both $\mathcal{N}(t)$ and $J(t)$ start to oscillate with the oscillations getting severe in the strong coupling regime. Since the measure of non-Markovianity measures the degree of non-Markovianity, we can therefore say that the interaction strength controls the nature of the dynamics, whether Markovian or non-Markovian.

In Fig. 4, we observe the behavior measure of non-Markovianity $\mathcal{N}(t)$ and von Neumann entropy [17,48] $\mathcal{S}(t)$,

$$S(t) = -\mathrm{Tr}(\rho \log_2 \rho) = -\sum_i \lambda_i \log_2 \lambda_i$$
$$= \log_2 \left\{ \left(\frac{1}{n(t)} - 1 \right)^{n(t)} \Big/ (1 - n(t)) \right\}, \qquad (50)$$

as time approaches infinity. The initial state is a pure state of the fermion of interest $\rho_S(0) = \rho(0) \otimes \rho_c(0) = d^\dagger|0\rangle\langle 0|d \otimes |0\rangle\langle 0| = d^\dagger|0\rangle\langle 0|d = \rho(0)$ whose von Neumann entropy evolves to the completely mixed state, the thermal equilibrium state, as time approaches infinity. Being a measure of loss of information, the graph of von Neumann entropy $\mathcal{S}(t)$, shows the leak of information [17,48] from the initial value of zero to the maximum of 1. Upon reaching the maximum value of 1, the graph of $\mathcal{S}(t)$ changes direction meaning that information starts flowing back, but it does not reach zero meaning that not all information flows back, rather it again starts leaking out to the mesoscopic bath again. This process repeats over and over with the amplitude of backflow reducing as thermalization is approached. On the other hand, the initial negative slope in the measure of non-Markovianity $\mathcal{N}(t)$ indicates loss of information [18] to the mesoscopic bath. The graph of $\mathcal{N}(t)$ reaches value of 1 where the von Neumann entropy is maximum and switches to positive slope indicating backflow to the site of interest. Like $\mathcal{S}(t)$, $\mathcal{N}(t)$ does not reach the previous point indicating that not all information flows back before it starts to leak to the mesoscopic bath. Thus, we observe a similar behavior in the two curves except that the directions are reversed. For pure initial states (like this particular case), existing literature [17,48,49] shows that the von Neumann entropy of the density matrix for either subsystem of a bipartite system can serve as a convenient measure of entanglement. Just as the initial pure state has zero von Neumann entropy which increases to maximum for a completely mixed state, it has zero entanglement which attains a maximum for a completely mixed state. Since fluctuations in entropy are in general caused by fluctuations in the

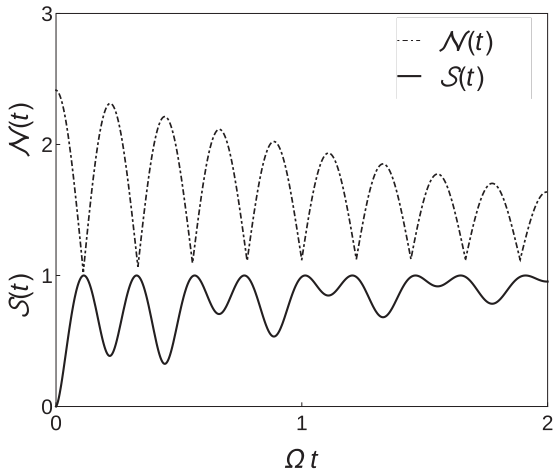

FIG. 4. Time dependence of measure of non-Markovianity $\mathcal{N}(t)$ and von Neumann entropy $\mathcal{S}(t)$; t is time measured in units of Ω^{-1} so that Ωt in the abscissa is dimensionless. All parameters are chosen to be the same for all curves: $g = 10$, $\epsilon = 1$, $\omega = 1.3$, $N = 5000$, $\Omega = \frac{\gamma}{2} = \pi J(\lambda_0) = \pi J(\lambda_1) = 10^{-6}$, and $\beta = 1$. The initial pure state of the fermion of interest evolves to the mixed state, the thermal equilibrium state, as time approaches infinity. Being a measure of loss of information, von Neumann entropy $\mathcal{S}(t)$ shows the leak of information from the initial value of zero to the maximum whereupon it starts flowing back, but does not all flow back, rather it again starts leaking out to the mesoscopic bath. On the other hand, the initial negative slope in the measure of non-Markovianity $\mathcal{N}(t)$ indicates loss of information to the mesoscopic bath. It reaches where the von Neumann entropy is maximum and switches to positive slope indicating backflow to the site of interest. It also does not reach the previous point. This process repeats over and over with the amplitude of backflow reducing as thermalization is approached.

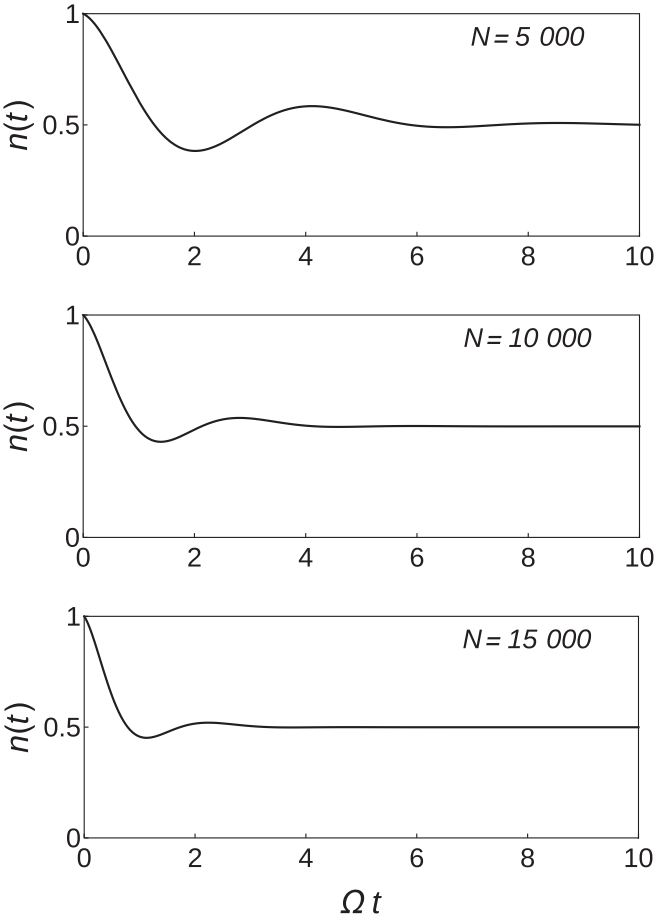

FIG. 5. Time dependence of mean number of the fermion of interest $n(t)$ for different values of number of fermions N in the mesoscopic bath; t is time measured in units of Ω^{-1} so that Ωt in the abscissa is dimensionless. The rest of the parameters are chosen to be the same for all three curves: $\epsilon = 1$, $\omega = 1.3$, $g = 1$, $\Omega = \frac{\gamma}{2} = \pi J(\lambda_0) = \pi J(\lambda_1) = 10^{-6}$, and $\beta = 1$.

temperature, we deduce that the cause of backflow is linked to fluctuations in the temperature and entanglement between the fermion of interest and the mesoscopic bath.

In Fig. 5, we analyze the influence of the number of fermions in the mesoscopic bath on the dynamics of the fermion of interest. From the top curve to the bottom one, the number of fermions in the reservoir is 5000, 10 000, and 15 000, respectively. The rest of the parameters are chosen to be the same for all three curves: $\epsilon = 1$, $\omega = 1.3$, $g = 1$, $\Omega = \frac{\gamma}{2} = \pi J(\lambda_0) = \pi J(\lambda_1) = 10^{-6}$, and $\beta = 1$. First of all, we note that we are in the strong coupling regime, hence the observed oscillations as explained above. It is clear from Fig. 5 that increasing the number of fermions in the mesoscopic bath leads to a faster decay to thermal equilibrium. Increased number of fermions in the mesoscopic bath means that the number of interactions with the fermion of interest is increased. In addition, the nature of the interactions is dissipative, so we expect faster decay to thermal equilibrium.

In Fig. 6, the mean number of fermions is plotted against time and the inverse temperature. The top curve corresponds to the value of β of 0.1, the middle one 1.0, and 10 the bottom one. The rest of the parameters are chosen to be the same: $\epsilon = 1$, $\omega = 1.3$, $g = 1$, $N = 5000$, and $\Omega = \frac{\gamma}{2} = \pi J(\lambda_0) = \pi J(\lambda_1) = 10^{-6}$. We note that all the three curves are exactly the same despite the differences in temperature leading us to observe that provided all other parameters are the same, the dynamics is independent of the temperature of the Markovian bath.

Figures 7 and 8 show graphs pertaining to our investigation of the behavior of the current density with time for different values of the number of fermions in the mesoscopic bath and for different temperatures of the Markovian bath.

In Fig. 7, we analyze the influence of the number of fermions in the mesoscopic bath on the current density. From the top curve to the bottom one, the number of fermions in the mesoscopic bath is 5000, 10 000, and 15 000, respectively. The rest of the parameters are chosen to be the same for all three curves: $\epsilon = 1$, $\omega = 1.3$, $g = 1$, $\Omega = \frac{\gamma}{2} = \pi J(\lambda_0) = \pi J(\lambda_1) = 10^{-6}$, and $\beta = 1$. Being in the strong coupling regime, we observe oscillations in all three curves, but the decay to $J(t) = 0$ is faster for increased number of fermions.

In Fig. 8, the current density is plotted against time for different values of inverse temperature of the mesoscopic bath. The top curve corresponds to the value of β of 0.1, the middle one 1.0, and 10 the bottom one. The rest of the parameters are chosen to be the same: $\epsilon = 1$, $\omega = 1.3$, $g = 1$, $N = 5000$, and $\Omega = \frac{\gamma}{2} = \pi J(\lambda_0) = \pi J(\lambda_1) = 10^{-6}$. We

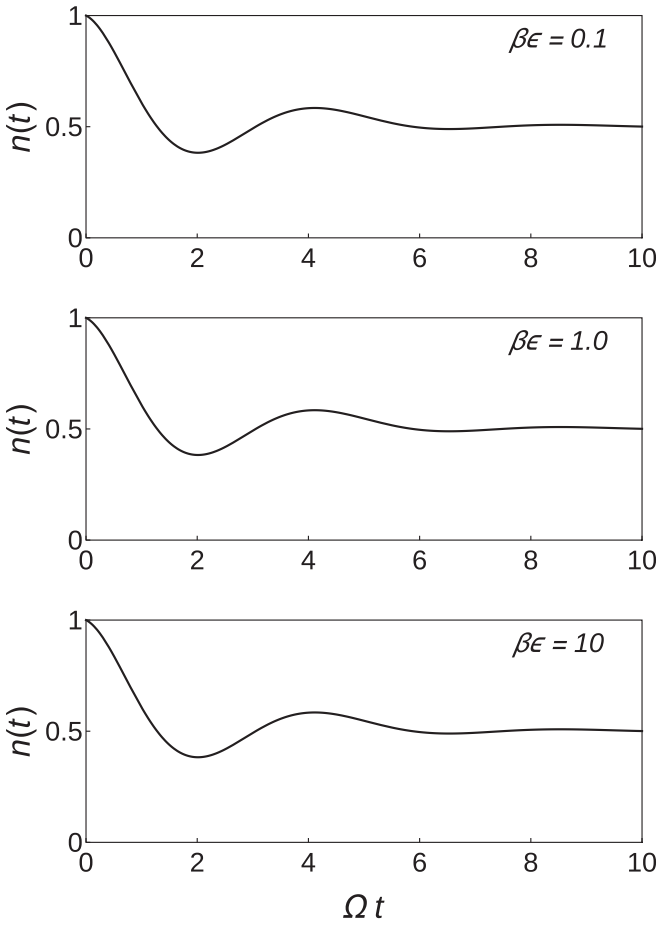

FIG. 6. Time dependence of the mean number of the fermion of interest $n(t)$ for different values of the inverse temperature β of the Markovian Bath; t is time measured in units of Ω^{-1} so that Ωt in the abscissa is dimensionless. The rest of the parameters are chosen to be the same: $\epsilon = 1$, $\omega = 1.3$, $g = 1$, and $\Omega = \frac{\gamma}{2} = \pi J(\lambda_0) = \pi J(\lambda_1) = 10^{-6}$.

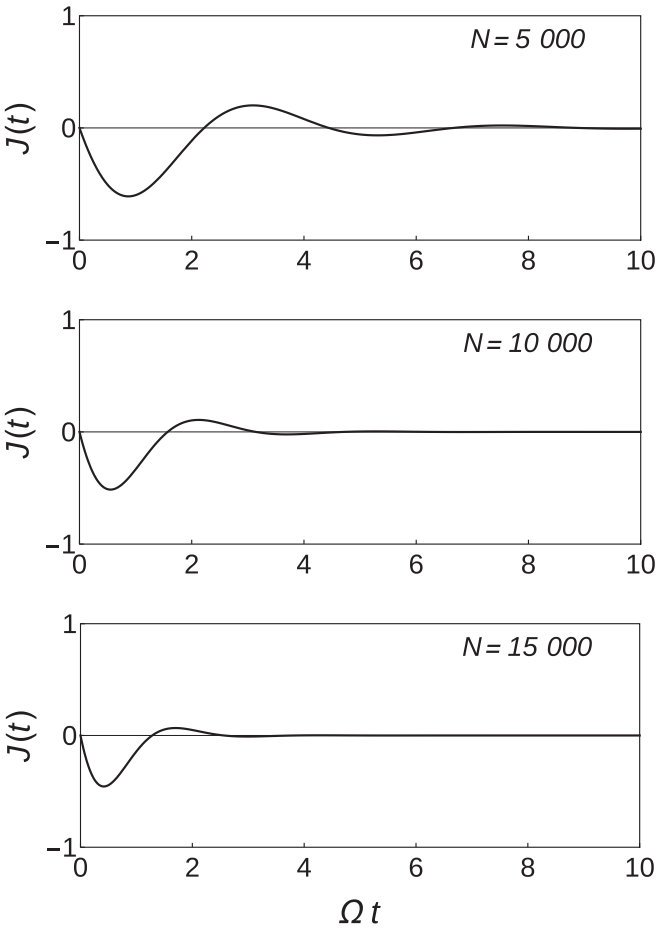

FIG. 7. Time dependence of current density $J(t)$ as a function of number of fermions N in the mesoscopic bath; t is time measured in units of Ω^{-1} so that Ωt in the abscissa is dimensionless. The rest of the parameters are chosen to be the same for all curves: $\epsilon = 1$, $\omega = 1.3$, $g = 1$, and $\Omega = \frac{\gamma}{2} = \pi J(\lambda_0) = \pi J(\lambda_1) = 10^{-6}$.

note that all three curves are exactly the same despite the differences in temperature leading us to a similar observation as our investigation of the behavior of the number of fermions in Fig. 6: Provided all other parameters are the same, the dynamics is independent of the temperature of the Markovian fermionic bath.

B. Thermalization of the fermion of interest

Our analysis of the dynamics of the mean number of fermions in the previous subsection as depicted in Fig. 2 to Fig. 8 shows thermalization as time approaches infinity. That observation was based on the graphs alone. In this subsection, we are going to show thermalization analytically.

Using the well-known canonical thermal equilibrium state [1],

$$\rho_{TS} = \frac{e^{-\beta H_S}}{Z}, \tag{51}$$

where $Z = \mathrm{Tr}(e^{-\beta H_S})$ is the normalizing partition function, the mean number of the fermion of interest in thermal equilibrium is

$$n_{TS} = \langle d^\dagger d \rangle = \mathrm{Tr}[d^\dagger d \rho_{TS}] = \frac{\mathrm{Tr}(d^\dagger d e^{-\beta H_S})}{\mathrm{Tr}(e^{-\beta H_S})}. \tag{52}$$

Substituting the system Hamiltonian, Eq. (9) and Eq. (18) into Eq. (52), we obtain

$$\begin{aligned} n_{TS} &= \frac{e^{-\beta\lambda_0}\cos^2\theta + e^{-\beta(\lambda_0+\lambda_1)} + e^{-\beta\lambda_1}\sin^2\theta}{(1+e^{-\beta\lambda_0})(1+e^{-\beta\lambda_1})} \\ &= p_0\cos^2\theta + p_1\sin^2\theta, \end{aligned} \tag{53}$$

where p_0 and p_1 are given by Eq. (31). Equation (53) is the expected mean number of the fermion of interest in thermal equilibrium.

On the other hand, our deductions from the previous subsection that thermalization is achieved as time approaches infinity imply that if we take the limit $t \to \infty$ in our calculations, Eq. (45), we should be able to get the expression for the thermal equilibrium mean number. Taking the limit $t \to \infty$ in Eq. (45), we get

$$n(\infty) = p_0\cos^2\theta + p_1\sin^2\theta, \tag{54}$$

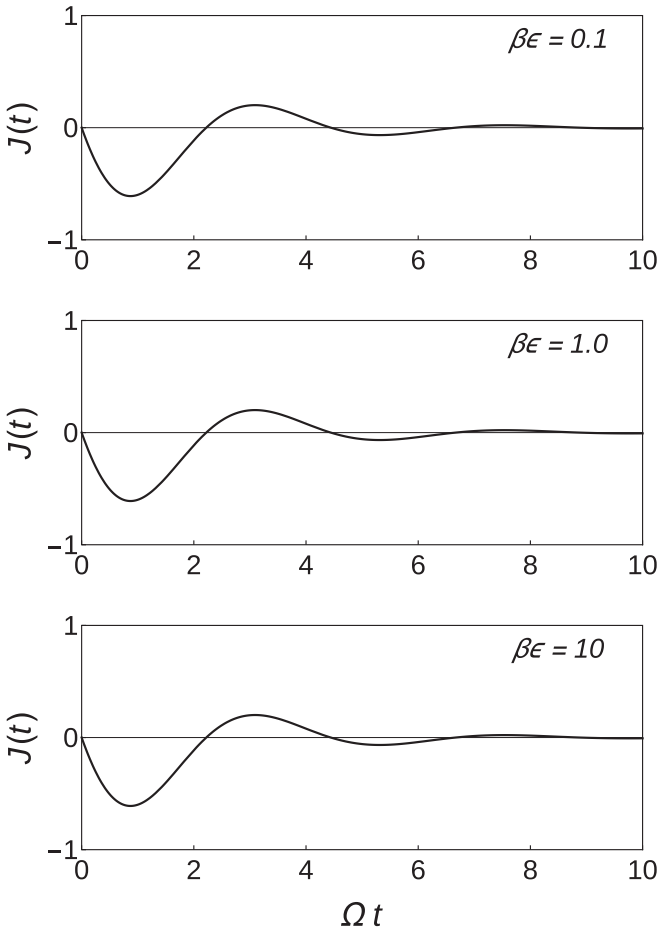

FIG. 8. Time dependence of the current density $J(t)$ for different values of the inverse temperature β of the Markovian Bath; t is time measured in units of Ω^{-1} so that Ωt in the abscissa is dimensionless. The rest of the parameters are chosen to be the same for all curves: $\epsilon = 1$, $\omega = 1.3$, $g = 1$, $N = 5000$, and $\Omega = \frac{\gamma}{2} = \pi J(\lambda_0) = \pi J(\lambda_1) = 10^{-6}$.

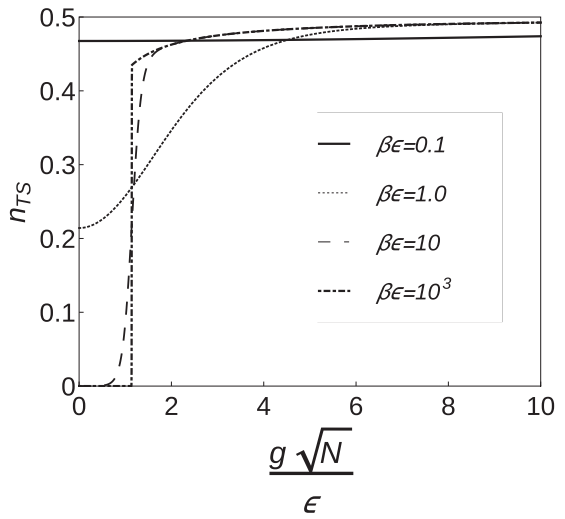

FIG. 9. Thermal state mean number as a function of the inverse temperature β and the dimensionless effective coupling strength $g\sqrt{N}/\epsilon$ and for values of $\epsilon = 1$, $\omega = 1.3$, $J(\lambda_0) = J(\lambda_1)$.

which is exactly the same as the expected thermal equilibrium mean number, Eq. (53). This indicates that thermalization is indeed achieved as time approaches infinity. The equality of the derived thermal equilibrium mean number and the expected thermal equilibrium mean number also gives us confidence in the approach and detailed derivations conducted in this work.

In Fig. 9, we analyze the dependence of the thermal equilibrium mean number on the inverse temperature, hence the temperature, of the Markovian bath and the effective coupling strength $g\sqrt{N}$. We observe that as $\beta \to 0$, i.e., for high temperatures of the Markovian bath, $n_{TS} \to 0.5$. This is exactly as expected from Eq. (53) where $p_i = 1/(1 + e^{\beta\lambda_i})$ given in Eq. (31) goes to 0.5 as $\beta \to 0$ resulting in $n_{TS} \to 0.5(\cos^2\theta + \sin^2\theta) = 0.5$. This is also exactly the same thermal mean number that we observed in the previous subsection. On the other hand, in the low-temperature regime, as $\beta \to \infty$, $p_i = 1/(1 + e^{\beta\lambda_i}) \to 0$ therefore $n_{TS} \to 0$. These observations can be explained as follows. When the temperature of the Markovian bath is low, its thermal energy and that of the mesoscopic bath is correspondingly low since the entire system is in thermal equilibrium. But the fermion of interest has higher energy when it is in its own subsystem than when it is in the subsystem of the mesoscopic bath, i.e., $\omega = 1.3 > \epsilon = 1$, and therefore can tunnel to the mesoscopic bath in one direction only leading to the average value of zero number of fermions of interest. For low temperatures of the Markovian bath and strong coupling strength, the tunneling is in both directions between the site of interest and the mesoscopic bath. This leads to the number of fermions of interest which was initially one being averaged between the two subsystems (fermion of interest and the mesoscopic bath), some kind of "sharing" of the single initial fermion of interest with the mesoscopic bath which initially had zero fermions. When the Markovian bath is at high temperatures, it supplies energy to the fermion of interest which has tunnelled to the mesoscopic bath and therefore can now tunnel back to the subsystem of the fermion of interest again resulting in the number of fermions of interest which was initially one averaged between the two subsystems. In the high-temperature regime, the same explanation holds regardless of the coupling regime hence the straight line corresponding to $\beta = 0.1$.

In Fig. 10, we observe similar behavior as in Fig. 9 except that now we have the difference between the energy of the fermion of interest and the energy of each of the fermions in the mesoscopic bath, $\Delta = (\omega - \epsilon)/\epsilon$, instead of the inverse temperature. At resonance (when $\omega = \epsilon$) or near resonance, the fermion of interest tunnels back and forth the mesoscopic bath rapidly with increasing coupling strength leading to a rapid attainment of the average value of one-half. In the far resonance when the fermion of interest has greater energy than the fermions in the mesoscopic bath, the rise to the average value of half is slow with increasing coupling strength because the back and forth tunneling is delayed: The fermion of interest has greater energy than the fermions in the mesoscopic bath and therefore its tunneling in one direction (toward the bath) is prolonged when the interaction strength is weak. As the coupling strength is increased, the fermions in the mesoscopic bath begin to tunnel back to the subsystem of the

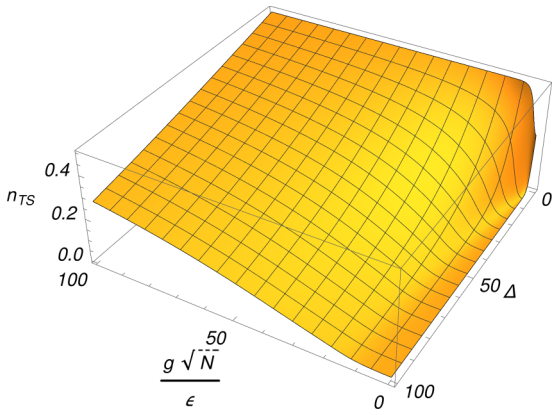

FIG. 10. Thermal state mean number as a function of the dimensionless effective coupling strength $g\sqrt{N}/\epsilon$ and dimensionless $\Delta = (\omega - \epsilon)/\epsilon$, measure of the difference between the energy of the fermion of interest and the energy of each of the fermions in the mesoscopic bath, for inverse temperature $\beta = 1, J(\lambda_0) = J(\lambda_1)$.

fermion of interest leading to attainment of the average value of one-half.

Let us now turn to the thermal state current density. From the expression for $J(t)$ in Eq. (47), we can calculate the expected thermal state current density by taking the limit $t \to \infty$:

$$J(\infty) = 0. \tag{55}$$

This can be compared with the value of the thermal state current density calculated explicitly from the thermal state density matrix:

$$J_{TS} = -i\mathrm{Tr}\{(c^\dagger d - d^\dagger c)\rho_{TS}\} = 0, \tag{56}$$

where ρ_{TS} is the thermal equilibrium state density matrix Eq. (51) and we have used the transformation equations, Eq. (18) and Eq. (19), for d and c, respectively. We see that $J(\infty)$ and J_{TS} are in exact agreement verifying that our system attains the state of thermal equilibrium after a long interval of time. This observation is also in line with the observations of Figs. 3–8 that the current goes to zero as time approaches infinity.

C. Thermal quantum correlations

In the previous subsection, we studied the properties of the thermal state of the fermion of interest. In the present section, we would like to extend the analysis to include the mesoscopic bath. Due to the symmetry of the model under consideration we have shown that effectively the fermion is coupled only to the symmetric collective mode $c = \frac{1}{\sqrt{N}}\sum_{i=1}^{N} c_i$. In this section, we analyze the thermal entanglement between fermion of interest and the collective fermionic mode of the mesoscopic bath c.

The explicit form of the Kraus operators Eq. (30) allows obtaining the joint density matrix of the fermion of interest and collective mode of the mesoscopic bath. These provide a direct way to analyze bipartite quantum correlations between the fermion of interest and the mesoscopic bath. However, the description of the entanglement in systems of fermions is not as straightforward as for systems of distinguishable two-level atoms [50,51]. These complications are arising from the indistinguishability and anticommutativity of the fermionic systems. In the present paper we will use entanglement of formation measure [51,52], which was adopted for the bipartite fermionic systems by Caban *et al.* [53] and applied to the description of the quantum correlations in the open fermionic systems [4,54].

Following Friis, Lee, and Bruschi [51], the entanglement of formation $\bar{E}(\rho)$ for fermionic systems is defined as

$$\bar{E}(\rho) = \min_{p_n, ||\psi_n\rangle\rangle} \sum_n p_n S(||\psi_n\rangle\rangle), \tag{57}$$

where the double-lined Dirac ket $||...\rangle\rangle$ denote the antisymmetrized state in the fermionic Fock space. The minimization is done over all fermionic pure state ensembles that realize the state $\rho = \sum_n p_n ||\psi_n\rangle\rangle\langle\langle\psi_n||$ with normalization $\sum_n p_n = 1$, $S(||\psi_n\rangle\rangle)$ denotes von Neumann entropy.

Caban *et al.* [53] has demonstrated that in the case of two fermions, one can construct mapping from two-fermion Fock space into $\mathbb{C}^2 \otimes \mathbb{C}^2$, such that the most general two-fermion density matrix obeying the fermion superselection rules reads

$$\rho = \begin{pmatrix} w_1 & 0 & 0 & b_1 \\ 0 & w_2 & b_2 & 0 \\ 0 & b_2^* & v_2 & 0 \\ b_1^* & 0 & 0 & v_1 \end{pmatrix}. \tag{58}$$

Nonzero coefficients of this matrix can be identified as the following expectation values,

$$\begin{aligned} w_1 &= \langle dd^\dagger cc^\dagger\rangle, \quad w_2 = \langle d^\dagger dcc^\dagger\rangle, \quad v_1 = \langle dd^\dagger c^\dagger c\rangle, \\ v_2 &= \langle d^\dagger dc^\dagger c\rangle, \quad b_1 = \langle c^\dagger d^\dagger\rangle, \quad b_2 = \langle c^\dagger d\rangle. \end{aligned} \tag{59}$$

In this case the entanglement of formation Eq. (57) reduces to

$$\bar{E}(\rho) = \sum_{i=1}^{2}(w_i + v_i)S_i, \tag{60}$$

where S_i is defined as

$$S_i = \begin{cases} 0, \text{ if } \quad w_i = v_i \quad \text{or} \quad b_i = 0, \\ -\frac{1-\xi_i}{2}\log_2\frac{1-\xi_i}{2} - \frac{1+\xi_i}{2}\log_2\frac{1+\xi_i}{2}, \end{cases} \tag{61}$$

and

$$\xi_i = \frac{w_i - v_i}{\sqrt{(w_i - v_i)^2 + 4|b_i|^2}}. \tag{62}$$

For the thermal state considered in this paper the coefficient $b_1 \equiv 0$. This leads to the following expression for the entanglement of formation,

$$\bar{E}(\rho) = -\langle d^\dagger d\rangle\left(\frac{1-\xi}{2}\log_2\frac{1-\xi}{2} + \frac{1+\xi}{2}\log_2\frac{1+\xi}{2}\right), \tag{63}$$

where the coefficient ξ is given by

$$\xi = \frac{\langle d^\dagger d\rangle - 2\langle d^\dagger dc^\dagger c\rangle}{\sqrt{(\langle d^\dagger d\rangle - 2\langle d^\dagger dc^\dagger c\rangle)^2 + 4|\langle d^\dagger c\rangle|^2}}, \tag{64}$$

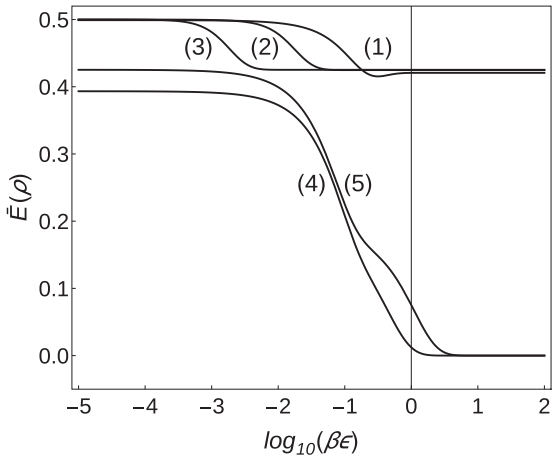

FIG. 11. Thermal entanglement of formation as the function of dimensionless inverse temperature ($\beta\epsilon$ in logarithmic scale). Curves (1)–(3) correspond to effective coupling strengths $g\sqrt{N} =$ (10, 100, 1000), respectively; the rest of the parameters are $\omega = 1.3$ and $\epsilon = 1$. Curves (4) and (5) correspond to the effective coupling strengths $g\sqrt{N} =$ (8, 10), while ω and ϵ are 13 and 10, respectively.

where the steady-state values of relevant observables are as follows:

$$\begin{aligned}\langle d^\dagger d\rangle &= \frac{p_0+p_1}{2} + \frac{p_0-p_1}{2}\frac{|\omega-\epsilon|}{\Omega_N},\\ \langle d^\dagger c\rangle &= \frac{g\sqrt{N}}{\Omega_N}(p_0-p_1),\\ \langle d^\dagger d c^\dagger c\rangle &= p_0 p_1.\end{aligned} \tag{65}$$

In Fig. 11 we show the thermal entanglement of formation Eq. (63) as the function of inverse temperature for various parameter regimes. We could clearly see that in the high-temperature regime ($\log\beta < 0$), the fermion of interest and the mesoscopic bath are thermally entangled. However, in the low temperature regime one can see two distinct behaviors. In one range of parameters the system remains entangled, while in the other regime there is no entanglement between the fermion of interest and the mesoscopic bath. In order to understand and explain this behavior we consider high-T and low-T limits of Eq. (63).

Using the explicit values of coefficients Eq. (65) we can analyze the high- and low-temperature behavior of the entanglement of formation for the studied system. The high-temperature expansion ($\beta\lambda_i \ll 1$) of the coefficients p_i reads

$$p_i \approx \frac{1}{2} - \frac{\lambda_i\beta}{4} + \frac{\lambda_i^3\beta^3}{48} + \ldots. \tag{66}$$

Substituting the high-temperature expansion for p_i in Eq. (64), the high-temperature expansion for ξ reads

$$\xi \approx \xi_{(0)} + \beta\xi_{(1)} + \ldots, \tag{67}$$

where the coefficients $\xi_{(i)}$ are given by

$$\xi_{(0)} = \frac{\min(\epsilon,\omega)}{\sqrt{4g^2N + \min(\epsilon,\omega)^2}}, \tag{68}$$

$$\xi_{(1)} = \frac{2g^2N(g^2N - \epsilon\omega)}{(4g^2N + \min(\epsilon,\omega)^2)^{3/2}}. \tag{69}$$

These lead to the high-temperature expansion of the entanglement of formation as follows,

$$\bar{E}(\rho) \approx \frac{S_0}{2} - \frac{\beta}{4}(\min(\omega,\epsilon)S_0 + S_1) + \ldots, \tag{70}$$

where

$$S_0 = -\frac{1-\xi_{(0)}}{2}\log_2\frac{1-\xi_{(0)}}{2} - \frac{1+\xi_{(0)}}{2}\log_2\frac{1+\xi_{(0)}}{2}, \tag{71}$$

and

$$S_1 = \xi_{(1)}\log_2\frac{1+\xi_{(0)}}{1-\xi_{(0)}}. \tag{72}$$

One could clearly see from Eq. (70) that for generic values of parameters of the system, in the high-temperature case there will always be some entanglement between the fermion of interest and the mesoscopic bath. The maximum value of thermal entanglement in the high-temperature limit is $\frac{1}{2}$; it follows from the fact that S_0 is bounded between 0 and 1. This behavior is clearly confirmed by curves depicted in Fig. 11.

In order to explain the difference in the low-T behavior between curves (1)–(3) and (4) and (5) in Fig. 11, one needs to consider the low-T limit case of Eq. (63). The low-temperature expansion of the coefficients p_i reads

$$\begin{aligned}p_0 &\approx e^{-\beta\lambda_0},\\ p_1 &\approx \begin{cases} e^{-\beta\lambda_1}, & \text{if} \quad \omega\epsilon > g^2N,\\ 1 - e^{-\beta|\lambda_1|}, & \text{if} \quad \omega\epsilon < g^2N.\end{cases}\end{aligned} \tag{73}$$

Substituting the above expansion in Eq. (64), one can obtain the expression for ξ:

$$\xi_{T=0} = \frac{\Omega_N - |\omega-\epsilon|}{\sqrt{(\Omega_N - |\omega-\epsilon|)^2 + 16g^2N}}. \tag{74}$$

Note that corrections ξ around $T = 0$ are exponentially small and can be neglected. These lead to the explicit expression for the entanglement of formation in the low-temperature limit,

$$\bar{E}(\rho) = \begin{cases} 0, & \text{if} \quad \omega\epsilon > g^2N,\\ \frac{1}{2}\left(1 - \frac{|\omega-\epsilon|}{\Omega_N}\right)S_{T=0}, & \text{if} \quad \omega\epsilon < g^2N,\end{cases} \tag{75}$$

where

$$\begin{aligned}S_{T=0} = &-\frac{1-\xi_{T=0}}{2}\log_2\frac{1-\xi_{T=0}}{2}\\ &-\frac{1+\xi_{T=0}}{2}\log_2\frac{1+\xi_{T=0}}{2}.\end{aligned} \tag{76}$$

The derived expression for the entanglement of formation at $T = 0$ Eq. (75) explains the qualitative difference in the behavior between curves (1)–(3) and (4) and (5) in Fig. 11. The curves (1)–(3) in Fig. 11 are in the range of parameters for which $\omega\epsilon < g^2N$, while curves (4) and (5) correspond to

the case $\omega\epsilon > g^2N$. This transition in the behavior is identical to the mean number of fermions just below and above the Fermi surface in the zero-temperature case. The entanglement of formation will have the Heaviside function behavior at the point $\omega\epsilon = g^2N$. Physically, the behavior can be explained as follows: In the case of $\omega\epsilon > g^2N$ the fermion of interest and the collective mode of the mesoscopic bath are in a localized state. Due to the nature of the interaction with the fermionic sea H_{SB} at the zero temperature all excitations from the mesoscopic bath are transferred to the fermionic sea. As a result the steady-state populations of the fermion of interest and the collective mesoscopic mode are zero, which leads to zero entanglement. In the case $\omega\epsilon < g^2N$ the fermion of interest and the collective mesoscopic mode are in two delocalized states and one of them is decoupled from the fermionic sea. This leads to nonzero populations in the steady-state and thermal entanglement at zero temperature.

IV. SUMMARY AND CONCLUSION

We have been studying the dynamics and thermalization of a spinless fermion embedded in the mesoscopic bath of spinless fermions which is in turn embedded in a fermionic Markovian bath. We made a number of assumptions. First, we considered the fermions in the mesoscopic bath to be degenerate and their coupling to the fermion of interest the same. These assumptions were taken in order to simplify the calculations while focusing on the dynamics. On the other hand, we noted that the model can be mimicked in an experimental setup. Such an experimental setup can be realized in the versatile platform of ultracold atoms in optical lattices which offers an unprecedented degree of controllability and flexibility in the preferred geometry [20,37,55,56]. The expressions for the interaction in the Hamiltonian Eq. (2) and Eq. (8) were based on the rotating wave approximation [44]. We started the derivations of the quantum master equation from the general expression for the quantum master equation, Eq. (25), in the Born-Markov approximation [1]. Finally, the derived quantum master equation, Eq. (26), holds in the case where $N \gg 1$.

Various plots for the mean number, the current density and thermal entanglement were obtained: Figs. 2–11, which allowed us to investigate the dynamics and thermalization of the fermion of interest. The plots for the mean number or current density against the coupling strength, Fig. 2 or Fig. 3, respectively, were monotonically decreasing in the weak coupling regime, and oscillating but exponentially decaying in the strong coupling regime. As confirmed in the literature [1,3,5,18], the behavior exhibited in the weak coupling regime is Markovian signifying irreversible flow of information from the subsystem of the fermion of interest to the mesoscopic bath while that of the strong coupling regime is non-Markovian where information also flows back into the subsystem of the fermion of interest. The curves for the BLP measure of non-Markovianity confirmed this observation. As a further investigation of the loss of information from the site of interest to the mesoscopic bath, we calculated the von Neumann entropy which was plotted in Fig. 4 on the same graph and with the same parameters as the BLP measure of non-Markovianity. Comparison of the two curves confirmed the above mentioned directionality of information flow and linked the cause of backflow to fluctuations in correlations (entanglement) between the fermion of interest and the mesoscopic bath. In probing thermalization, it was observed that in both the weak and strong coupling regimes, the behavior of the graphs against time of the mean number, current density, non-Markovianity measure, and von Neumann entropy is such that thermalization is achieved for long times. As a verification for thermalization, analytical calculations for both the mean number of the fermion of interest and the current density, Eqs. (53) and (54), and Eqs. (55) and (56), respectively, were performed confirming that thermalization is indeed achieved as time approaches infinity. Keeping all parameters the same, the graphs of the mean number or current density against the coupling strength, Fig. 2 or Fig. 3, respectively, show that the stronger the coupling the more rapid the thermalization process. Keeping all parameters the same and varying only the number of fermions in the mesoscopic bath, thermalization is more rapid for an increased number of fermions (Figs. 5 and 7). However, keeping all parameters the same, variations in the temperature of the Markovian bath displayed no effect on the rate of thermalization; neither do variations in the temperature of the Markovian bath induce any switch from Markovian to non-Markovian dynamics or vice versa (Figs. 6 and 8).

The thermal mean number was also investigated with variations in both the coupling strength and temperature of the Markovian bath (Figs. 9 and 10). We found that the switch from Markovian dynamics to non-Markovian dynamics or vice versa, is controlled by the coupling strength. The results of this work display behavior which is expected from literature [1,3,5–7,17]. Figure 11 shows thermal entanglement of formation as the function of inverse temperature (in logarithmic scale). One could see that in the high-temperature regime the fermion of interest is entangled with the collective mode of the mesoscopic bath. This is also confirmed by the high-temperature expansion of the expression for the entanglement of formation Eq. (70). In the low-temperature case, the sudden death of entanglement is observed [57]. The analytical calculations of the zero-temperature thermal entanglement of formation predict nonzero quantum correlations for the $\omega\epsilon < g^2N$ and zero entanglement otherwise Eq. (75). These predictions are in perfect agreement with cases depicted in Fig. 11. Thus, we have been able to link the cause of non-Markovian behavior to fluctuations in entanglement (quantum correlations) which is strongly dependent on the coupling strength. It also becomes strongly dependent on temperature in the thermal state. In the future we plan to take into account spin-spin interactions and consider more general initial conditions.

ACKNOWLEDGMENTS

This work is based upon research supported by the South African Research Chair Initiative of the Department of Science and Technology and National Research Foundation of South Africa. I.S. acknowledge support in part by the National Research Foundation of South Africa (Grant No. 119345).

[1] H.-P. Breuer and F. Petruccione, *The Theory of Open Quantum Systems* (Oxford University Press, Oxford, 2002).

[2] S. Bhattacharya, A. Misra, C. Mukhopadhyay, and A. K. Pati, Phys. Rev. A **95**, 012122 (2017).

[3] Z. Man, N. B. An, and Y. Xia, Opt. Express **23**, 5763 (2015).

[4] J. Cheng, W. Z. Zhang, Y. Han, and L. Zhou, Phys. Rev. A **91**, 022328 (2015).

[5] T. J. Barreiro, Nat. Phys. **7**, 927 (2011).

[6] S. Ajisaka, F. Barra, C. Mejía-Monasterio, and T. Prosen, Phys. Rev. B **86**, 125111 (2012).

[7] D. S. Kosov, T. Prosen, and B. Žunkovič, J. Phys.: Condens. Matter **25**, 075702 (2013).

[8] V. V. Sargsyan, G. G. Adamian, N. V. Antonenko, and D. Lacroix, Phys. Rev. A **90**, 022123 (2014).

[9] A.-M. Visuri, J. J. Kinnunen, J. E. Baarsma, and P. Törmä, Phys. Rev. A **94**, 013619 (2016).

[10] A. Karmakar and G. Gangopadhyay, Phys. Scr. **85**, 045008 (2012).

[11] P. Hedegard and A. O. Caldeira, Phys. Rev. B **35**, 106 (1987).

[12] S. Camalet, Eur. Phys. J. B **61**, 193 (2008).

[13] P. W. Anderson, Phys. Rev. **124**, 41 (1961); U. Fano, *ibid.* **124**, 1866 (1961).

[14] A. J. Leggett, S. Chakravarty, A. T. Dorsey, M. P. A. Fisher, A. Garg, and W. Zwerger, Rev. Mod. Phys. **59**, 1 (1987).

[15] U. Weiss, *Quantum Dissipative Systems*, 2nd ed., Series in Modern Condensed Matter Physics, Vol. 10 (World Scientific, Singapore, 1999).

[16] A. O. Caldeira and A. J. Leggett, Ann. Phys. **149**, 374 (1983).

[17] M. A. Nielsen and I. L. Chuang. *Quantum Computation and Quantum Information*, 10th Anniversary Edition (Cambridge University Press, Cambridge, 2010).

[18] H.-P. Breuer, E.-M. Laine, and J. Piilo, Phys. Rev. Lett. **103**, 210401 (2009).

[19] B. Bylicka, D. Chruściński, and S. Maniscalco, Sci. Rep. **4**, 5720 (2014).

[20] S. McEndoo, P. Haikka, G. De Chiara, G. M. Palma, and S. Maniscalco, Europhys. Lett. **101**, 60005 (2013).

[21] J. F. Poyatos, J. I. Cirac, and P. Zoller, Phys. Rev. Lett. **77**, 4728 (1996).

[22] A. Sarlette, J. M. Raimond, M. Brune, and P. Rouchon, Phys. Rev. Lett. **107**, 010402 (2011).

[23] I. Sinayskiy, E. Ferraro, A. Napoli, A. Messina, and F. Petruccione, J. Phys. A **42**, 485301 (2009).

[24] F. Anzà and V. Vedral, Sci. Rep. **7**, 44066 (2017).

[25] C. Ates, J. P. Garrahan, and I. Lesanovsky, Phys. Rev. Lett. **108**, 110603 (2012).

[26] H. Tasaki, Phys. Rev. Lett. **80**, 1373 (1998).

[27] J. Gemmer and G. Mahler, Eur. Phys. J. B **31**, 249 (2003).

[28] J. Gemmer, A. Otte, and G. Mahler, Phys. Rev. Lett. **86**, 1927 (2001).

[29] R. Vasile, S. Maniscalco, M. G. A. Paris, H. P. Breuer, and J. Piilo, Phys. Rev. A **84**, 052118 (2011).

[30] M. M. Wolf, J. Eisert, T. S. Cubitt, and J. I. Cirac, Phys. Rev. Lett. **101**, 150402 (2008).

[31] A. Rivas, S. F. Huelga, and M. B. Plenio, Phys. Rev. Lett. **105**, 050403 (2010).

[32] X.-M. Lu, X. Wang, and C. P. Sun, Phys. Rev. A **82**, 042103 (2010).

[33] S. Luo, S. Fu, and H. Song, Phys. Rev. A **86**, 044101 (2012).

[34] J. Wesenberg and K. Mølmer, Phys. Rev. A **65**, 062304 (2002).

[35] D. J. Wineland, J. J. Bollinger, W. M. Itano, and D. J. Heinzen, Phys. Rev. A **50**, 67 (1994).

[36] H.-P. Breuer, D. Burgarth, and F. Petruccione, Phys. Rev. B **70**, 045323 (2004).

[37] M. Köhl, H. Moritz, T. Stöferle, K. Günter, and T. Esslinger, Phys. Rev. Lett. **94**, 080403 (2005).

[38] W. Hofstetter, J. I. Cirac, P. Zoller, E. Demler, and M. D. Lukin, Phys. Rev. Lett. **89**, 220407 (2002).

[39] C. Honerkamp and W. Hofstetter, Phys. Rev. Lett. **92**, 170403 (2004).

[40] B. Paredes, C. Tejedor, and J. I. Cirac, Phys. Rev. A **71**, 063608 (2005).

[41] D. C. McKay and B. DeMarco, Rep. Prog. Phys. **74**, 054401 (2011).

[42] R. Onofrio, Phys. Usp. **59**, 1129 (2016).

[43] P. Diao, S. Deng, F. Li, A. Chenu, A. del Campo, and H. Wu, New J. Phys. **20**, 105004 (2018).

[44] B. Thimmel, P. Nalbach, and O. Terzidis, Eur. Phys. J. B **9**, 207 (1999).

[45] K. Kraus, States, *Effects and Operations* (Springer/Verlag, Berlin, 1983).

[46] H. Nakazato, Y. Hida, K. Yuasa, B. Militello, A. Napoli, and A. Messina, Phys. Rev. A **74**, 062113 (2006).

[47] S. Wißmann, A. Karlsson, E.-M. Laine, J. Piilo, and H.-P. Breuer, Phys. Rev. A **86**, 062108 (2012).

[48] N. Cerf and C. Adami, Physica D **120**, 62 (1998).

[49] W. K. Wootters, Phys. Rev. Lett. **80**, 2245 (1998).

[50] M.-C. Banuls, J. I. Cirac, and M. M. Wolf, Phys. Rev. A **76**, 022311 (2007).

[51] N. Friis, A. R. Lee, and D. E. Bruschi, Phys. Rev. A **87**, 022338 (2013).

[52] C. H. Bennett, D. P. DiVincenzo, J. A. Smolin, and W. K. Wootters, Phys. Rev. A **54**, 3824 (1996).

[53] P. Caban, K. Podlaski, J. Rembielinski, K. A. Smolinski, and Z. Walczak, J. Phys. A: Math. Gen. **38**, L79 (2005).

[54] J. Cheng, Y. Han, Q.-Z. An, and L. Zhou, Ann. Phys. **354**, 590 (2015).

[55] P. Haikka, S. McEndoo, G. De Chiara, G. M. Palma, and S. Maniscalco, Phys. Rev. A **84**, 031602(R) (2011).

[56] D. Jaksch, H. J. Briegel, J. I. Cirac, C. W. Gardiner, and P. Zoller, Phys. Rev. Lett. **82**, 1975 (1999).

[57] T. Yu and J. H. Eberly, Science **323**, 598 (2009).